

Structure of Polyelectrolytes in Poor Solvent

HANS JÖRG LIMBACH¹, CHRISTIAN HOLM¹ and KURT KREMER¹

¹ *Max-Planck-Institut für Polymerforschung, Ackermannweg 10, 55128 Mainz, Germany*

PACS. 61.25.Hq – Macromolecular and polymer solutions.

PACS. 36.20.Ey – Polymer molecules - conformation.

PACS. 87.15Aa – Theory and modeling; computer simulation.

Abstract. – We present simulations on charged polymers in poor solvent. First we investigate in detail the dilute concentration range with and without imposed extension constraints. The resulting necklace polymer conformations are analyzed in detail. We find strong fluctuations in the number of pearls and their sizes leading only to small signatures in the form factor and the force-extension relation. The scaling of the peak in the structure factor with the monomer density shows a pertinent different behavior from good solvent chains.

Polyelectrolytes (PEs) are polymers that carry ionizable groups that dissociate ions in aqueous solution. Technical applications range from viscosity modifiers, precipitation agents, superabsorbers to leak protectors [1]. In biochemistry and molecular biology they are of great importance because virtually all proteins, as well as DNA, are PEs.

Many PEs contain a non-polar hydrocarbon backbone, for which water is a poor solvent. Therefore, in aqueous solution, there is a competition between the tendency to precipitate, the Coulomb interaction and the entropic degrees of freedom. This can lead to elongated strings of locally collapsed structures (pearls). Such necklace conformations have been predicted on the basis of scaling arguments in ref. [2] for a weakly charged single chain PE, and have been confirmed by simulations using the Debye-Hückel approximation [3] and with explicit counterions [4,5]. However, there is up to now no clear experimental evidence for the existence of necklace chains [6, 7]. Using extensive computer simulations of poor solvent PEs we find an extended coexistence regime between different necklace structures that smears out the necklace signatures, which is one reason why these conformations are so difficult to detect. In clear contrast to good solvent PEs we find that the peak in the structure factor of the solution scales proportional to the density $\rho^{1/3}$ from the dilute up into the dense phase.

Our PE model consists of a bead spring chain of Lennard-Jones (LJ) particles, whose interaction at distance $r < R_c$ is given by $U^{LJ}(r) = 4\epsilon[(\frac{\sigma}{r})^{12} - (\frac{\sigma}{r})^6 - c]$, and is zero elsewhere. The constant c is chosen such that the potential value is zero at the cutoff R_c , and ϵ is a measure of the solvent quality. Chain monomers interact up to a distance $R_c = 2.5\sigma$ and experience an attraction with $\epsilon = 1.75k_BT$, which is deep in the poor solvent regime. The Θ -point for this model is at $\epsilon = 0.34k_BT$ [4]. The counterions interact via a purely repulsive interaction with $R_c = 2^{1/6}\sigma$. The units of length, energy and time are σ , ϵ , and τ , respectively (LJ units). For bonded monomers we add a FENE potential of the form $U^F(r) =$

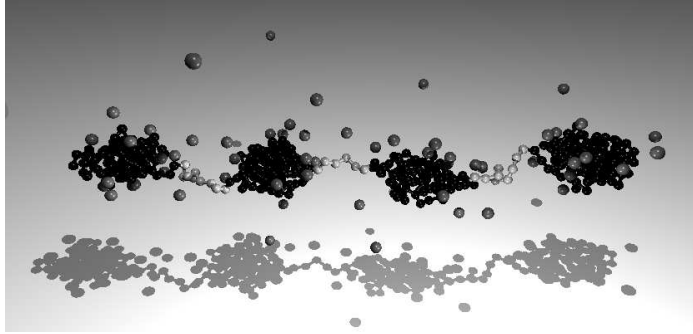


Fig. 1 – Snapshot of a necklace structure analyzed with the cluster algorithm. Chain length $N_m = 382$: (black) monomers in pearls, (light gray) monomers in strings, (gray) counterions.

$-\frac{1}{2}k_F R_0^2 \ln(1 - (\frac{r}{R_0})^2)$, with $k_F = 7.0 \frac{k_B T}{\sigma^2}$ and $R_0 = 2\sigma$, which results in an average bond length $b = 1.09\sigma$. Charged particles at separation $r_{ij} = |\mathbf{r}_j - \mathbf{r}_i|$ interact via the Coulomb energy $E^C(r_{ij}) = k_B T \ell_B q_i q_j / r_{ij}$, with $q_i = 1, (-1)$ for the charged chain monomers (counterions). The Bjerrum length $\ell_B = e^2 / (4\pi\epsilon_S\epsilon_0 k_B T)$ (e : unit charge, ϵ_0 and ϵ_S : permittivity of the vacuum and of the solvent) is set to $\ell_B = 1.5\sigma$. A velocity Verlet algorithm with a standard Langevin thermostat is used to integrate the equation of motion [8] (friction coefficient $\Gamma = \tau^{-1}$, time step $\Delta t = 0.0125\tau$). After equilibrating we measured for about 10^7 time steps in each case. The Coulomb interaction was calculated with the P3M-algorithm [9], tuned to force accuracies well above the thermal noise level. The central simulation box of length L contained $N_P = 5, 10$ or 32 chains subject to periodic boundary conditions. Each chain consisted of $N_m = 48 \dots 478$ monomers, with a charge fraction $f = 1/3 \dots 1/2$. Other parameter sets yield qualitatively similar results [10, 11], so that we restrict ourselves here to the above described “generic” system. Due to criticisms one finds in the literature about the equilibration of NVT simulations we have checked our systems in several ways. For the longest chains the simulation time is around 200 times the measured correlation time for the End-to-end distance R_E . In all simulations the chains centers of mass diffuse at least several R_G . Using simulations at different densities we find that the pressure p is always positive and that the pV diagram is convex at all densities. This shows that our simulations are stable, reach true thermal equilibrium and reside in a one phase region. Especially they are not trapped in meta-stable states, which in some cases we also checked by using different initial conditions. The volume density inside the pearls does not exceed 0.47, which is well below the glass transition.

Being first interested in single chain properties we used a monomer density $\rho_m = (N_P N_m) / L^3 = 1.5 \times 10^{-5} \sigma^{-3}$. A typically 4-pearl (and 3-string) structure is shown in fig. 1. The substructures contain 90-8-94-6-77-9-98 monomers. For the identification of the pearls and strings we used an especially adapted cluster algorithm [10, 11].

Most quantities will be discussed for chains of length $N_m = 430$, where we find structures with 4, 5, 6 and 7 pearls and a mean pearl number of $\langle n_P \rangle = 5.22$. Other chain lengths can be found in table I. The coexistence regime between different structure types increases with increasing chain length. One reason for the small differences in the free energy is the interplay between the chain conformation and the counterion distribution. Conformations with a lower number of pearls have on average a smaller extension, e.g. R_E , and a larger pearl size. This leads to a stronger attraction of counterions towards the chain and yields a smaller effective charge on the chain which in turn stabilizes larger pearl sizes and smaller chain

TABLE I – *Basic observables for various chain lengths under dilute conditions. Types denotes the observed structures with n_P pearls, and angular brackets denote the time and ensemble averaged values for the distance between neighboring pearls r_{PP} and the number of monomers g_P in a pearl. δr_{PP} and δg_P denote the relative standard deviations. p and Π are the pressure and the osmotic coefficient respectively. $\rho_m = 1.48 \times 10^{-5} \sigma^{-3}$, $\ell_B = 1.5\sigma$, $f = 1/3$.*

N_m	$R_E [\sigma]$	$\langle n_P \rangle$	Types	$\langle r_{PP} \rangle [\sigma]$	δr_{PP}	$\langle g_P \rangle$	δg_P	$p [10^{-6} k_B T \sigma^{-3}]$	Π
46	3.48	1.0	1	-	-	48	0.0	4.79	0.96
142	12.9	1.97	2	11.6	0.16	67.5	0.17	2.97	0.59
238	25.4	2.89	2 - 4	12.8	0.20	75.5	0.30	2.31	0.46
334	30.4	3.94	3 - 5	13.1	0.21	78.6	0.33	2.0	0.40
382	45.4	4.53	3 - 6	13.3	0.22	78.0	0.32	1.75	0.35
430	55.4	5.22	4 - 7	13.2	0.22	75.3	0.35	1.78	0.36
478	79.7	5.60	4 - 7	13.3	0.21	78.3	0.34	1.76	0.35

extensions. In contrast to scaling theories [12–15] we do not find a collapse into a globular state due to this effect. This is consistent with a more refined theoretical analysis [16] that takes prefactors and finite concentrations into account. The interplay between counterion distribution and structural changes of the conformation can be measured e.g. via the number of counterions $n_c(n)$ for a n pearl structure inside a shell of 3σ from the chain. For the example we have $n_c(4) = 60.4$, $n_c(5) = 56.7$, $n_c(6) = 52.8$ and $n_c(7) = 50.2$. From the probability $p(n)$ of finding a n pearl structure we can calculate the free energy difference $\Delta\mathcal{F}^{nm} = k_B T \ln(p(n)/p(m))$. We find $\Delta\mathcal{F}^{45} = -1.33k_B T$, $\Delta\mathcal{F}^{56} = 0.66k_B T$, $\Delta\mathcal{F}^{67} = 1.90k_B T$, which are all of the order $k_B T$ explaining the observed large coexistence regime. On order to exclude the possibility of metastable states for our parameters, we have observed the time evolution for a single chain. We find typically many transitions between different structure types, see i.e. one example for $N_m = 430$ in fig. 2. Not only the pearl number, also the position and size of the pearls fluctuate strongly. For chains with more than 2 pearls, both the mean values as well as the relative standard deviations δ of the distance r_{PP} between neighboring pearls and

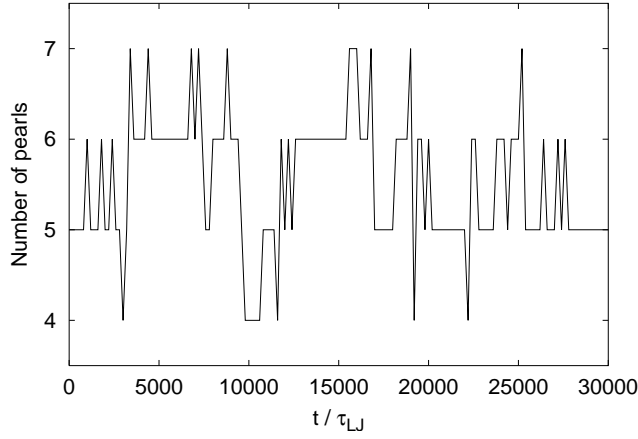


Fig. 2 – Time evolution of a single chain of length $N_m = 430$ in equilibrium, shown over a quarter of the physical running time. Many transitions between different structure types can be observed.

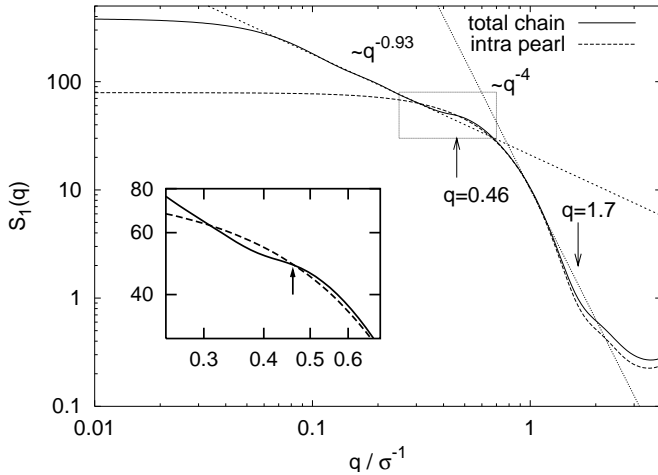


Fig. 3 – Form-factor $S_1(q)$ for pearl necklaces: (solid) form-factor of the whole chain, (dashed) form-factor due to intra pearl scattering, (dotted) form-factor of an ideal necklace as described in the text. The marked region is enlarged in the inlay.

the number g_P of monomers in a pearl are almost constant, see table I, which is consistent with scaling theory.

Scattering experiments access the chain conformation via the chain form factor $S_1(q)$ given by

$$S_1(q) = \frac{1}{4\pi N_m} \left\langle \sum_{i,j=1}^{N_m} \frac{\sin(q r_{ij})}{q r_{ij}} \right\rangle, \quad (1)$$

where $\langle \dots \rangle$ denotes the ensemble average. An advantage of simulations is here the direct access to real space conformations. fig. 3 shows the form factor for $N_m = 382$ (see table I). In the Guinnier regime ($R_G q \ll 1$) the radius of gyration R_G can be calculated from $S_1(q) = N_m (1 - (R_G q)^2/3)$, giving $R_G = 16.8\sigma \pm 0.3\sigma$, in agreement with the directly calculated value $R_G = 16.9\sigma \pm 0.4\sigma$. In the range $0.07\sigma^{-1} \leq q \leq 0.3\sigma^{-1}$ S_1 scales as $q^{-0.93}$ which corresponds to a globally stretched object. Around $q = 0.46\sigma^{-1}$ the form factor has an inflection point. A comparison with the intra pearl scattering reveals that this is caused by inter pearl scattering (inlay in fig. 3). Dividing out the intra pearl form factor gives access to the inter pearl scattering and thus r_{PP} . The form factor yields $\langle r_{PP} \rangle = 13.6\sigma$, in good agreement with the directly measured value $\langle r_{PP} \rangle = 13.3\sigma$ (table I). In the region around $q = 1.0\sigma^{-1}$ we find $S_1(q) \propto q^{-4}$, the typical Porod scattering. From the small dip at $q = 1.7\sigma^{-1}$ one can calculate the radius r_P of the pearls to be $\langle r_P \rangle = 2.6\sigma$ which again compares well to the real space value $\langle r_P \rangle \simeq 3\sigma$. We conclude that the cooperative effect of fluctuations on overlapping length scales broadens all characteristic signatures which can be revealed by scattering under experimental conditions (polydispersity, charge fluctuations, etc). Thus they might be difficult to detect.

The overall scattering function $S(q)$ of the solution contains additional experimental information. We analyze here the inter chain scattering $S_{IC} = S/S_1$. For good solvent PEs experiments [17], theory [18], and simulations [19] find a pronounced first peak of S_{IC} at $q^* = (2\pi)/\xi$, where ξ is the correlation length. The position varies as $q^* \propto \rho_m^{1/3}$ in the very dilute regime and crosses over to a $\rho_m^{1/2}$ regime at higher concentrations. In fig. 4 we have

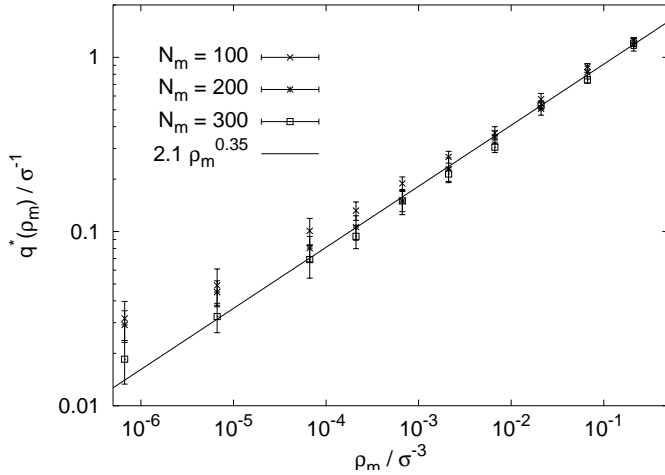


Fig. 4 – Density dependence of the peak q^* in the structure factor for three different chain length $N_m = 100, 200, 300$ with $f = 0.5$. The black line is a fit to the data with $N_m = 200$.

plotted the density dependence of q^* in poor solvent for different chain lengths. Within the error bars we find that for poor solvent chains q^* scales proportional to $\rho_m^{0.35 \pm 0.04}$ for all concentrations. There are two reasons for this. First, due to the delicate balance between attractive and repulsive forces, the response of the polyelectrolyte conformation on density changes is much larger in the poor solvent case [4, 10] than in the good solvent case [19], and the chain extension behaves non-monotonic as a function of density [4, 10]. Second, in the density regime between $\rho_m = 10^{-2}\sigma^{-3} \dots 10^{-4}\sigma^{-3}$ the pearl number, and therefore the chain extension, changes dramatically upon changes in the density, and almost all monomers are located within the pearls. The pearls experience a strong intra and inter chain pearl-pearl repulsion. Thus one essentially observes the arrangement of repelling spheres, suggesting a $q^* \propto \rho_m^{1/3}$ power law. Upon approaching the dense regime, the string length tends to zero and we find a chain of touching pearls. Our result is compatible to scaling exponents found in scattering experiments [20].

Scaling theories [13, 21] have predicted a $\rho_m^{1/2}$ regime to start at ρ_o^* , which is defined at the density where $R_e \approx \xi$, and to extend until $\xi \approx r_{PP}$ where the bead-controlled $\rho_m^{1/3}$ regime starts. We find $\rho_o^* \simeq 5 \times 10^{-2}, 10^{-3}, 10^{-4}$ for $N_m = 100, 200, 300$, and r_{PP} is equal to ξ between $\rho_m = 10^{-2}$ and 10^{-1} . One probable reason for our different findings is the strong inter-chain coupling and influence of the counterions on the conformations which are not sufficiently taken into account in the mean field approach. It is not clear at this stage if the $\rho_m^{1/2}$ regime can be recovered for much longer chain length. In addition we observe that the chains form a transient physical network which has neither been seen in previous simulational studies nor predicted by theoretical approaches. During the simulation time these networks reconstruct several times, e.g. chains are not trapped towards each other as one might suspect due to the strong hydrophobic attraction.

A different way to measure a distinct signature of the pearls is given by single-molecule force spectroscopy, e.g. stretching the chain by AFM [22] or optical tweezers. The case of an imposed end-to-end distance was investigated in Refs. [14, 23, 24] for a weakly charged chain at infinite dilution, for which a pronounced saw-tooth pattern in the force-extension curve

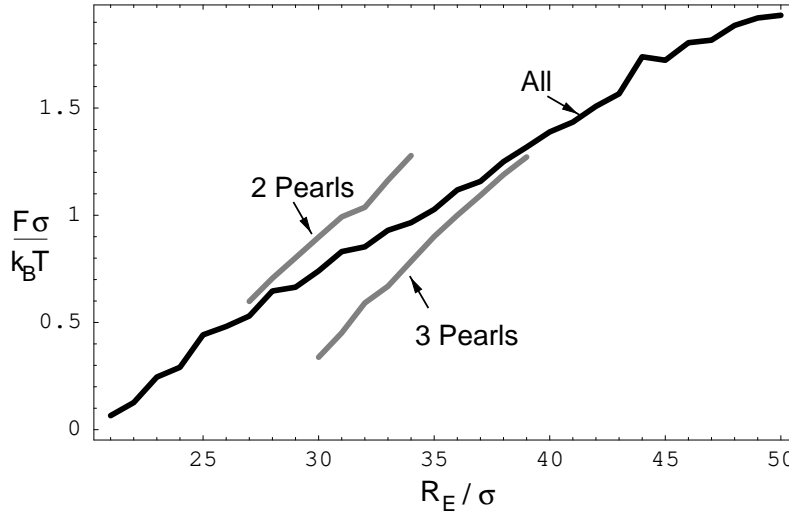


Fig. 5 – Force-extension relation for a transition from two to three pearls. Shown are the average over all conformations, over only two-pearl configurations and only three-pearl configurations.

was found. To investigate this situation we performed simulations in the weak coupling limit, using a single chain with $N_m = 256$, $f = 1$, $\ell_B = 0.08\sigma$, and no counterions present.

At equilibrium this system is in a two-pearl configuration with an end-to-end distance $R_E = 21\sigma$. To measure the force-extension curve we simulated a large number of systems with a fixed end-to-end distance up to $R_E = 50\sigma$. For each end-to-end distance the force on the end-monomers was measured, yielding a continuous curve (Fig. 5). The first remarkable observation is that the two-pearl state evolves into a three-pearl state under extension, which was predicted in ref. [23, 24]. This is counter intuitive from simple arguments, but can be shown to result from the electrostatic inter-pearl interactions [10]. Only when the force averages where computed separately for the three- and two-pearl states, we recognize the predicted saw-tooth pattern in the force. In equilibrium one would expect a rounded plateau for the transition, and the upper and lower part would correspond to metastable superheated and supercooled states. Again, due to the large fluctuations all nontrivial signatures in the force-extension relation are washed out. Analyzing the variance of the measured forces by applying a time window of the order of the transition time we find a 25% increase in the width of the force distribution in the transition region $R_E = 30 \dots 34\sigma$, and a bimodal force distribution. This means that one needs an experimental time resolution below one μs to directly resolve the structure dependent force difference. An estimate of typical viscous and inertial forces acting on colloidal particles shows that the Brownian motion of small spheres attached to a single PE chain might indeed reflect the fluctuating forces exerted by the chains. The experimental determination of these fluctuating forces by optical nanorheology [25] or AFM noise analysis [26] presumably is difficult due to the high characteristic frequencies involved.

To sum up we find that poor solvent PEs show an extended coexistence regime between different necklace structures. We observe stable necklaces even with condensed counterions. In all investigated cases the signatures of necklaces in the chain form factor are broadly smeared out. A similar broadening of signatures is found for the force-extension curve which will obscure any of the recently predicted saw-tooth patterns [14, 23, 24]. Nevertheless, the simulations reproduce the predicted initial increase of pearl number under imposing an external

length constraint [23, 24]. Our results suggest that the strong fluctuations impose a severe obstacle in observing necklace structures and structural transitions directly in experiments. Finally, as a result of the special chain conformations, the location of the first peak in the solution structure factor is qualitatively different from that of PEs in good solvent. This is in accordance to experiments [6] but does not show the full complexity of the proposed scaling picture at this point [21].

* * *

We thank B. Dünweg, D. Johannsmann, B. Mergell, H. Schiessel and M. Tamashiro for many fruitful discussions and comments. A large computer time grant hkf06 from NIC Jülich is also gratefully acknowledged.

REFERENCES

- [1] *Polyelectrolytes: Science and Technology*, edited by M. Hara (Marcel Dekker, New York, 1993).
- [2] A. V. Dobrynin, M. Rubinstein, and S. P. Obukhov, *Macromolecules* **29**, 2974 (1996).
- [3] A. V. Lyulin, B. Dünweg, O. V. Borisov, and A. A. Darinskii, *Macromolecules* **32**, 3264 (1999); P. Chodanowski and S. Stoll, *J. Chem. Phys* **111**, 6069 (1999).
- [4] U. Micka, C. Holm, and K. Kremer, *Langmuir* **15**, 4033 (1999).
- [5] U. Micka and K. Kremer, *Europhys. Lett.* **49**, 189 (2000).
- [6] M. D. Carbalal-Tinoco and C. E. Williams, *Europhys. Lett.* **52**, 284 (2000); T. A. Waigh, R. Ober, C. E. Williams, and J.-C. Galin, *Macromolecules* **34**, 1973 (2001).
- [7] M. Heinrich *et al.*, *Eur. Phys. J. E* **4**, 131 (2001); V. O. Aseyev *et al.*, *Macromolecules* **34**, 3706 (2001).
- [8] G. S. Grest and K. Kremer, *Phys. Rev. A* **33**, 3628 (1986).
- [9] M. Deserno and C. Holm, *J. Chem. Phys.* **109**, 7678 (1998); **109**, 7694 (1998).
- [10] H. J. Limbach, Ph.D. thesis, Johannes Gutenberg Universität, Mainz, Germany, 2001. <http://www.mppip-mainz.mpg.de/theory.html>
- [11] H. J. Limbach and C. Holm, in preparation (2002).
- [12] H. Schiessel and P. Pincus, *Macromolecules* **31**, 7953 (1998).
- [13] A. V. Dobrynin and M. Rubinstein, *Macromolecules* **32**, 915 (1999).
- [14] T. A. Vilgis, A. Johner, and J.-F. Joanny, *Eur. Phys. J. E* **2**, 289 (2000).
- [15] A. Khokhlov, *J. Phys. A* **13**, 979 (1980).
- [16] M. Deserno, *Eur. Phys. J. E* **6**, 163 (2001).
- [17] M. Nierlich *et al.*, *J. Physique* **40**, 701 (1979); M. Drifford and J.-P. Dalbiez, *J. Phys. Chem.* **88**, 5368 (1984); K. Kaji, H. Urakawa, T. Kanaya, and R. Kitamaru, *J. Physique* **49**, 993 (1988); L. Wang and V. Bloomfield, *Macromolecules* **24**, 5791 (1991).
- [18] J. F. Joanny, in *Electrostatic effects in Soft Matter and Biophysics*, Vol. 46 of *NATO Science Series II - Mathematics, Physics and Chemistry*, edited by C. Holm, P. Kékicheff, and R. Podgornik (Kluwer Academic Publishers, Dordrecht, NL, 2001), pp. 149–170.
- [19] M. J. Stevens and K. Kremer, *J. Chem. Phys.* **103**, 1669 (1995).
- [20] W. Essafi, F. Lafuma, and C. E. Williams, *J. Phys. II* **5**, 1269 (1995); M. N. Spiteri, F. Boue, A. Lapp, and J. P. Cotton, *Physica B* **234**, 303 (1997).
- [21] A. V. Dobrynin and M. Rubinstein, *Macromolecules* **34**, 1964 (2001).
- [22] T. Hugel *et al.*, *Macromolecules* **4**, 1039 (2001).
- [23] M. N. Tamashiro and H. Schiessel, *Macromolecules* **33**, 5263 (2000).
- [24] G. T. Pickett and A. C. Balazs, *Langmuir* **17**, 5111 (2001).
- [25] T. Gisler and D. A. Weitz, *Curr. Opin. Colloid Interface Sci.* **3**, 586 (1998).
- [26] M. Gelbert, M. Biesalski, J. Rühe, and D. Johannsmann, *Langmuir* **16**, 5774 (2000).